



Snow Depth Estimation on Lead-less Landfast ice using Cryo2Ice satellite observations

Monojit Saha¹, Julienne Stroeve^{1,2}, Dustin Isleifson¹, John Yackel³, Vishnu Nandan^{1,3}, Jack Landy⁴, Hoi Ming Lam³

5 1Centre for Earth Observation Science, Department of Environment and Geography, University of Manitoba, Winnipeg, Canada

2 Department of Earth Sciences, University College London. London, United Kingdom

3 Department of Geography, University of Calgary, Calgary, Canada

4 Centre for Integrated Remote Sensing and Forecasting for Arctic Operations (CIRFA), UiT The Arctic University of Norway, Tromsø, Norway

Correspondence to: Monojit Saha (saham1@myumanitoba.ca)

Abstract. Observations of snow on Arctic sea ice are vitally important for sea ice thickness estimation as well as for understanding bio-physical processes and human-activities. This study is the first assessment of the potential for near-coincident ICESat-2 and Cryosat-2 (Cryo2Ice) snow depth retrievals in a lead-less region of the Canadian Arctic Archipelago. Snow depths are retrieved using the absolute difference in surface height from a near-coincident ICESat-2 and Cryosat-2 after applying an ocean tide correction between satellite passes 77 minutes apart. Both the absolute mean snow depths and snow depth distributions retrieved from Cryo2Ice compare favourably to in-situ measurements. All four in-situ sites had snow with saline basal layers and different levels of roughness/ridging. The retrieved Cryo2Ice snow depths were underestimated by an average of 20.7 % which is slightly higher than the tidal adjustment applied. Differences in the Cryo2Ice and in-situ snow depth distributions reflected the different sampling resolutions between the sensors and the in-situ measurements, with more heavily ridged areas producing larger mean underestimation of the snow depth. Results suggest the possibility of estimating snow depth over lead-less landfast sea ice but attributing 2-3 cm biases to differences in sampling resolution, snow salinity, density, surface roughness and/or errors in altimeter's tidal corrections require further investigation.

25 1 Introduction

Changes in Arctic sea ice are affecting climate, ecosystems and traditional ways of living and harvesting (Meier and Stroeve, 2022). A critical component of the sea ice cover is its overlying snow cover, which has been challenging to accurately measure by satellites (Webster et al., 2018). Snow acts as an insulator, impacting both the growth and decay of sea ice (Maykut and Untersteiner, 1971). Snow also (1) limits the amount of light penetrating through the sea ice, affecting the timing of sea ice algae growth (Mundy et al., 2005); (2) contributes to the amount of freshwater discharged to the ocean, affecting its budget (Andersen et al., 2019); and (3) affects the heat exchange between the atmosphere and the sea ice (Andreas et al., 2005).



Using coincident airborne laser and radar altimeter data collected during the Laser-Radar Altimetry (LaRA) mission over sea ice around Svalbard, Leuschen et al., 2008, suggested snow depth could be retrieved by differencing freeboards, though there was a lack of in-situ ground truth to validate results. Following this, studies have differenced coincident satellite radar (CryoSat-2; hereafter CS2) and laser (ICESat-2; hereafter IS2) altimeter freeboards to estimate pan-Arctic (e.g. Kwok and Markus, 2018; Kwok et al., 2020) and Antarctic snow depth (Kacimi and Kwok, 2020). However, significant uncertainties remain related to (1) differences in electromagnetic frequencies and spatial resolution (Fons et al., 2021), (2) whether or not the CS2 Ku-band radar returns originate from the snow/ice interface, which has been contested even for a dry and cold (below freezing) snow pack (Willatt et al., 2011; Nandan et al., 2017; de Rijke Thomas et al., 2023), (3) the influence of surface roughness over different length scales on the laser and radar waveforms (Landy et al., 2019) and (4) spatial heterogeneity of snow distributed over sea ice.

Earlier studies also faced challenges of having different orbits for CS2 and IS2, limiting the number of exact footprint crossovers (Kwok & Markus, 2018). Kwok and Markus (2018) made a case for adjusting the CS2 orbit to achieve more overlaps with IS2, thereby improving both spatial and temporal coincidence. As part of the Cryo2Ice campaign, the CS2 orbit was raised by ~ 900 meters in August 2020 to significantly increase the amount of IS2 crossovers (ESA, 2020). This realignment means that once in every 19 CS2 (20 IS2) cycles, the two ground track nearly align for a few hundred kilometers over the Arctic.

With the Cryo2Ice campaign, new opportunities are possible to improve and validate snow depths retrieved by combining laser and radar freeboards. This study provides the first high-resolution in-situ validation of snow depths retrieved along coincident Cryo2Ice tracks on the 29th of April 2022 (29-04-2022) near Cambridge Bay, Nunavut in the Canadian Arctic Archipelago (CAA). The CAA is a region with significantly different bathymetry and icescape than the Central Arctic (Galley et al., 2012). Sea ice in the CAA is landfast ice for the majority of the year (6 to 8 months) (Melling, 2002), and exhibits minimal ice drift (Galley et al., 2012). The tidal amplitudes within the shallow bathymetry of the CAA are also much larger than in the open ocean. This poses additional challenges compared to validation studies in the Central Arctic Ocean. The most prominent challenge is the lack of open water for estimating the local sea surface height (SSH) needed to reference the freeboards. Landfast ice grows along the narrow channels in the CAA and often lacks leads for several hundred kilometers (Galley et al., 2012). Therefore, assuming IS2 and CS2 are viewing the same landfast ice, the variation in SSH due to tidal variations must be known and corrected between the two sensors. Our objective is to develop an approach to combine IS2 and CS2 along-track data in regions where the local SSH estimate is not readily available from local observations. The along-track CS2/IS2 retrieved snow depths are then validated using near-coincident in-situ snow depth observations. We further use in-situ snow property observations and satellite estimates of the surface roughness to examine the drivers of CS2 and IS2 height variability. Finally, the sources of bias in the retrieval process and major challenges are discussed.



2 Data and Methods

2.1 ICESat-2 (IS2)

65 The Advanced Topographic Laser Altimeter System (ATLAS) is the photon counting LiDAR system onboard ICESat-2. ATLAS emits low-energy 532 nm (green) pulses in three two-beam pairs which have a cross track spacing of 3.3 km between each pair with intra-pair spacing of 90 meters. The laser has a footprint size of 11 meters (Magruder et al., 2020). Detailed specifications can be found in Neumann et al., (2019).

In this study, the uncorrected ATL07 Sea Ice Height Release Version 6 available from the National Snow and Ice Data Centre
70 (<https://nsidc.org/data/atl07ql/versions/6#anchor-2>) is used, which provides uncorrected sea ice heights computed directly from ATL03 photo heights. Sea ice heights within the 25 km land-buffer are included despite low confidence in the geophysical corrections close to land (Kwok et al., 2023). The strong beam (gt2l) from ATL07 is used based on proximity to the CS2 reference ground track and field sampling sites.

The ATL07 geophysical corrections are summarized in Table A1. Each correction is time-varying and has different impacts
75 on the retrieved IS2 heights. The ocean tide corrections are provided every hour and can vary between ± 62 cm which is the largest among the different geophysical corrections applied. The ocean tide corrections are obtained from the Global Ocean Tide Model 4.8 (GOT 4.8) (Kwok et al., 2021). GOT 4.8 model provides tide predictions for all regions of the globe based on the assimilation of data from satellite altimetry and tide gauge measurements into a tidal model. Since the tidal corrections originate from different models between the two sensors with varying spatio-temporal resolutions, the accuracy of these
80 corrections varies regionally.

2.2 CryoSat-2 (CS2)

The SAR Interferometric Radar Altimeter (SIRAL) is the primary instrument on board CryoSat-2, which is a combination of a pulse-limited radar altimeter along with a Synthetic Aperture Radar (SAR) Interferometer system (SARIn). SIRAL operates at Ku-band (13.575 GHz) and in three different modes with along-track sampling resolution of around 300 m and across-track
85 resolution of 1600 m (ESA, 2013). Cryosat-2 operated in the SARIn mode in the CAA during the study period. Here we use the CS2 Level 2 Baseline E products available through the European Space Agency's EO-CAT web explorer (<https://eocat.esa.int/>). The CS2 Level 2 sea ice heights are re-tracked using the University College London (UCL) retracker (Tilling et al., 2018) which assumes a threshold on the first peak for diffuse echoes representing the mean elevation of the snow/sea ice interface within the footprint.

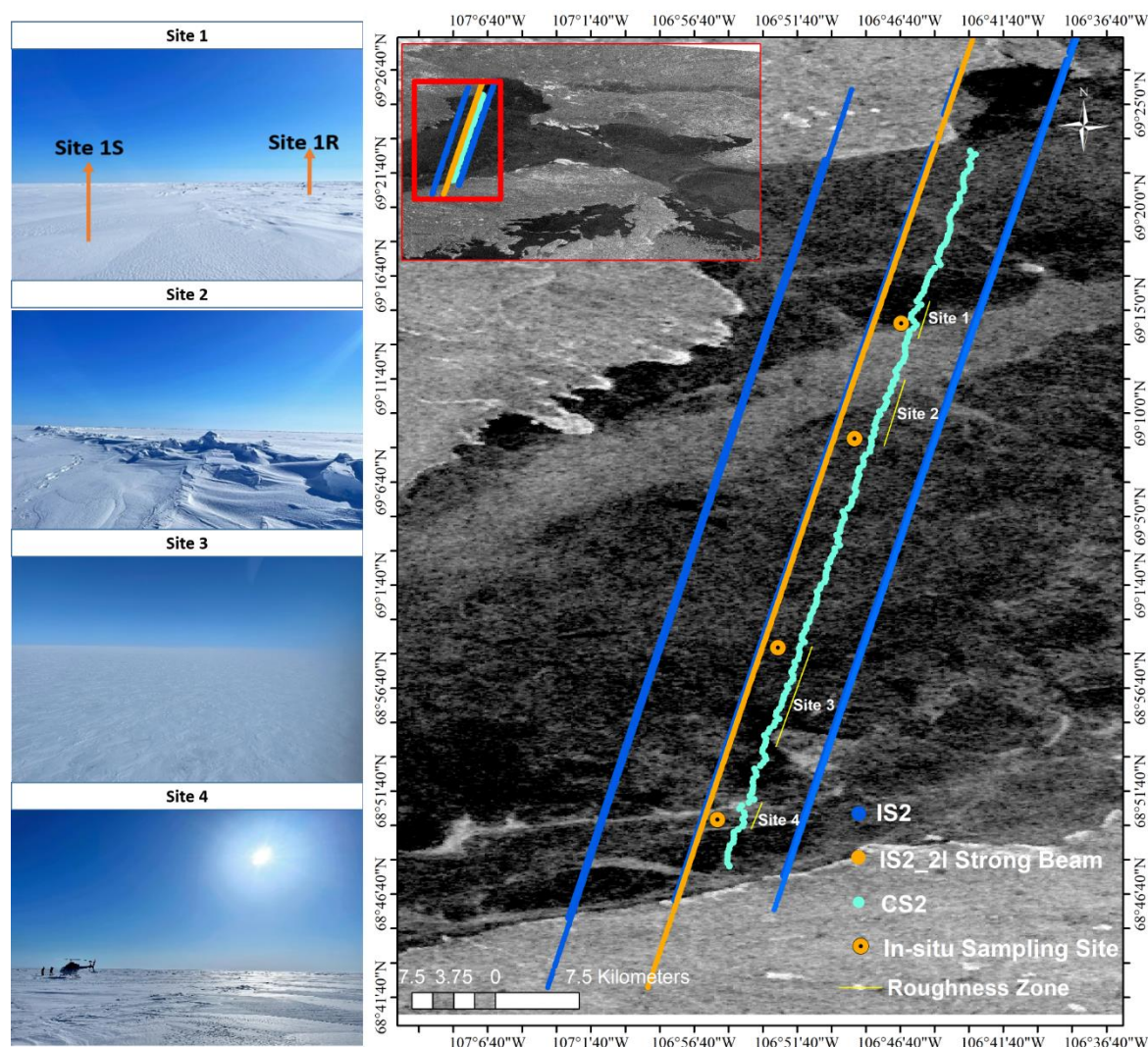
90 Tidal corrections (ocean, long-period equilibrium, ocean loading, solid earth and geocentric polar) are included in the Level 2 Baseline E Cryosat-2 SAR/SARIn product (Table B2). The ocean tide, long-period equilibrium tide and ocean loading tide corrections used are retrieved from the Finite Element Solution 2004 Ocean Tide Model (FES 2004) (Cryosat-2 Product Handbook). The ocean tide corrections typically range from ± 50 cm.



2.3 Field Measurements

95 The study site comprised a 75 km long NNE-to-SSW transect across Dease Strait ($69^{\circ}26'58.02''\text{N}$ $106^{\circ}41'57.25''\text{W}$ to $68^{\circ}46'42.48''\text{N}$ $106^{\circ}55'52.10''\text{W}$) (Figure 1), ~70 km west of Cambridge Bay, NU. This region connects Coronation Gulf and Queen Maud Gulf of the Kitikmeot Sea and is a part of the southern route of the Northwest Passage (Xu et al., 2021). Dease Strait is relatively shallow (maximum depth ~ 100 meters), and its narrow channel is covered by landfast ice normally between November and mid-July (Galley et al., 2012). CS2 and IS2 coincident tracks were identified using the CS2 and IS2 Coincident

100 Data Explorer (<https://cs2eo.org/>) (Ewart et al., 2022). The tracks were ~1.5 km apart and passing by within 77 minutes of each other (Figure 3).



105 **Figure 1** Map shows the Cryosat-2 Points of Closest Approach (POCA) locations, IS2 2I Strong Beam and other IS2 beam, in-situ sampling locations and identified roughness zones. The background contains Sentinel-1 HH-pol SAR imagery. Site photos show the variation in snow roughness.



In-situ snow depths were collected at four different sites (Sites 1-4) ranging from smooth, rough and mixed sea ice roughness zones. Based on Sentinel-1 SAR and field reconnaissance, Site 1 was classified as a rough and smooth sea ice transition zone; Site 2 was a thin snow zone with significant ridging; Site 3 was a smooth sea ice zone with extensive areas of thin snow; and Site 4 was a rough sea ice site with extensive areas of thick snow. All sites were located equidistant between the IS2 strong
110 beam and CS2 track to ensure the highest likelihood that snow depth sampling was representative of both sensors. The snow depth sampling direction was determined according to distinctive roughness features at individual sites, ensuring sufficient sampling distance in both the along- and across-track directions, representative of the prevailing east-southeast wind direction (ECCC, 2022) and snow dune pattern (Moon et al., 2019). Snow depth was surveyed using Snow-Hydro's automated snow depth magnaprobe, which has an accuracy of ± 0.3 cm on level sea ice and snow (Strum and Holmgren, 2018). The magnaprobe
115 was reassembled and re-calibrated before each sampling effort to avoid instrument bias. Sampling was conducted by a single person to avoid variations in instrument handling and to maintain constant intervals between samples.

All four sites were surveyed on 01-05-2022 within 48 hours of the ICESat-2 and Cryosat-2 pass on 29-04-2022. The sites were accessed via helicopter and no sampling was conducted within 200 meters of the helicopter landing zone to avoid snow redistribution during landing. The sampling interval was set at 5 m intervals to ensure spatial heterogeneity and avoid spatial
120 autocorrelation of the sampled snow depth values following (Iacozza and Barber, 1999). There was no precipitation recorded during the sampling period, nor during the time interval between the CS2 and IS2 overpasses. Furthermore, high pressure dominated the region between 26-04-2022 and 04-05-2022 causing light surface winds. As such, snow redistribution between CS2 and IS2 overpasses and in-situ sampling was negligible. The air temperature varied between -11.7°C and -14.1°C during the sampling as measured at the Cambridge Bay, land-based meteorological station.

Snow geophysical properties including snow salinity and density were sampled from all four sites. Snow temperature was not
125 measured because the temperature probe would not calibrate quickly enough between the short helicopter landing durations. For Site 1, two pits were sampled, one for the rough sea ice (Site 1a) and one for the relatively smooth sea ice zone (Site 1b). Single pits were excavated at the other three sites. Snow density was measured using a 66 cm^3 ($2 \times 5.5 \times 6$ cm) density cutter at 2 cm intervals and weighed in the lab. Weighed samples were then melted at room temperature for snow salinity
130 measurement using a Cole-Parmer C100 Conductivity Meter (accuracy of $\pm 0.5\%$). Sea ice thickness and freeboard at each site was measured using a freeboard tape to an accuracy of 0.5 cm.

2.4 Estimating Snow Depth from Cryosat-2 and ICESat-2

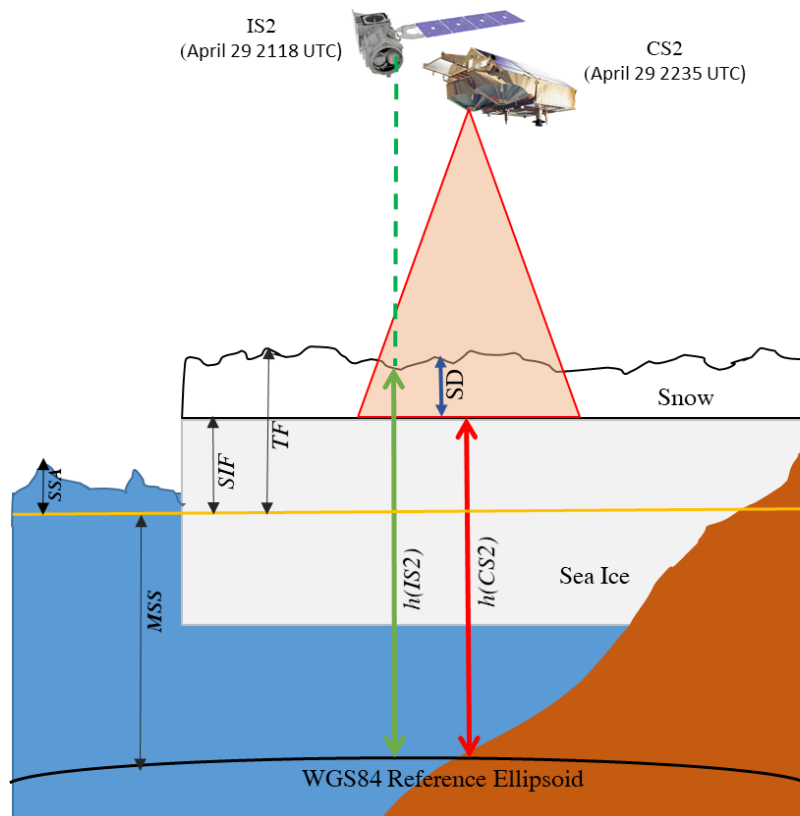
Kwok et al (2020) calculates snow depth (SD) as the difference between IS2-derived total freeboard (snow + ice) and CS2-
135 derived sea ice freeboard (CS2), using the difference between the surface height and the instantaneous sea surface height interpolated from sea surface measurements from along-track leads to obtain the freeboards (Kwok et al., 2020; Ricker et al., 2014). However, reliable freeboard measurements from IS2 and CS2 are dependent on accurate estimation of the sea surface height which is dependent on the availability of leads within a reasonable distance (10's of km) along both the IS2 and CS2 track. No leads were detected along the portion of the IS2 and CS2 tracks in the study area and therefore the sea surface height



could not be estimated. Therefore, we modified the approach used in Kwok et al., (2020). We used the absolute sea ice heights
 140 measured from IS2 ATL07 (hIS2) and CS2 (hCS2) referenced to the WGS84 ellipsoid to estimate SD (Figure 3). SD can be
 calculated as the freeboard differences under the assumption that Ku-band penetrates to the snow/ice interface

$$SD = \frac{h_{IS2} - h_{CS2}}{\eta_s}, \quad (1)$$

Where η_s is the refractive index of Ku-band microwaves which compensates for the propagation delay through the snow pack
 (Kwok et al., 2020). The refractive index is calculated using $(\eta_s = (1 + 0.51\rho_s)1.5)$ (Ulaby et al., 1986), where the in-situ bulk
 145 snow density (ρ_s) measured from the field is used. The average snow density from all four sites is used to compute snow depth
 for the entire track (Figure 8) while snow densities from each site are used to compute SD from corresponding portions of the
 Cryo2Ice track (Figure 5).



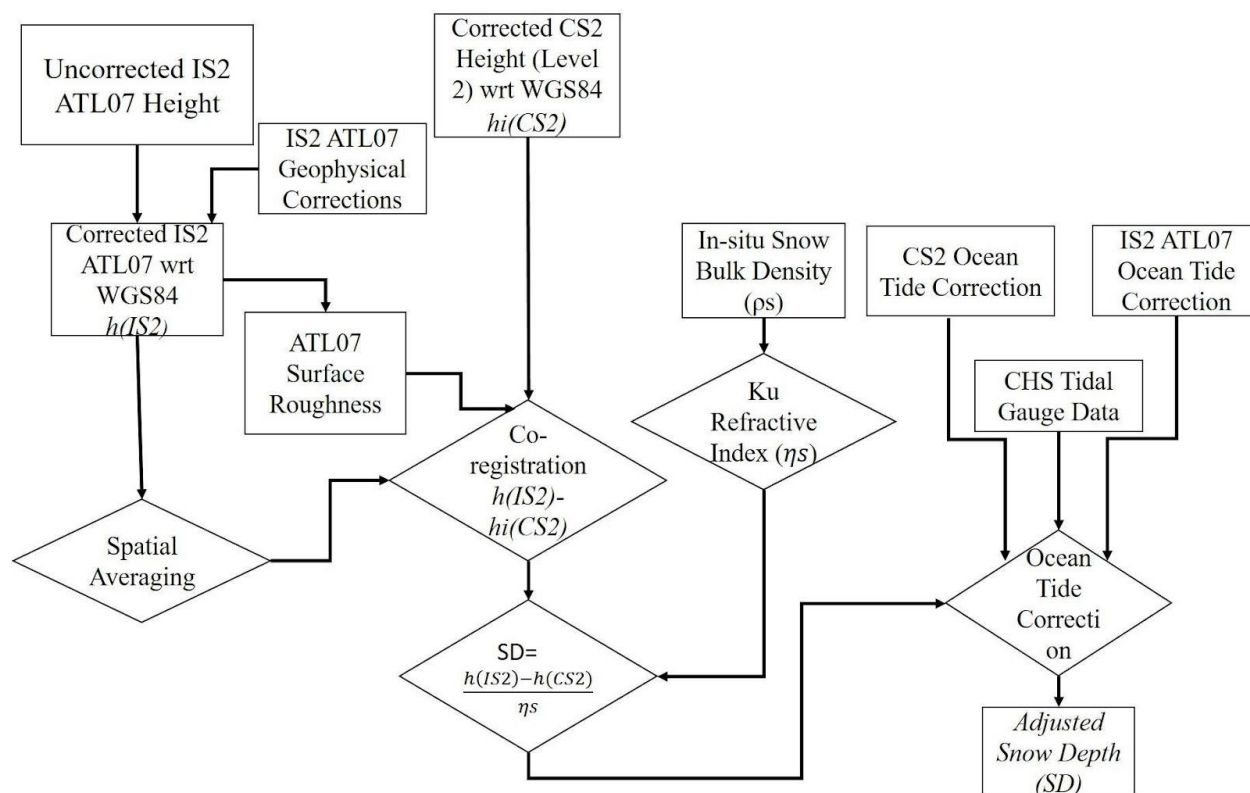
150 **Figure 2** Schematic showing the calculation of snow depth (SD) from ICESat-2 and Cryosat-2 over sea ice. The diagram illustrates the representative heights for the sea surface anomaly (SSA), mean sea surface (MSS) in yellow, sea ice freeboard (SIF) and total freeboard (TF). SD is shown with the blue arrow, IS2 surface height (h_{IS2}) is shown with the green arrow and CS2 surface height (h_{CS2}) is represented by the red arrow. Land is orange.



2.5 Data Processing

The uncorrected IS2 ATL07 heights (h (IS2)) are referenced to the WGS84 ellipsoid which is also consistent with the CS2
155 heights (Figure 2). The following geophysical corrections contained within the IS2 ATL07 product are applied to the ATL07
sea ice heights: ocean tide correction, long-period equilibrium tide and inverted barometer correction. However, the mean sea
surface (MSS) is not added for reasons explained in Section 2.6. The same geophysical corrections included within the CS2
product are applied to the CS2 L2 sea ice heights. However, there is limited confidence in these individual geophysical
corrections closer to land. Moreover, the tides varied over a range of ~ 6.0 cm in Dease Strait in between the two passes, so it
160 was crucial to check if the tidal corrections contained within the products accurately accounted for tide differences in the ~ 77
minutes between passes. Therefore, after comparing the geophysical correction as explained in Section 2.6, an ocean tide
correction factor is derived to account for the variation in SSH between the IS2 and CS2 acquisitions.

Both CS2 and IS2 have significantly different footprints (Section 2.1 and 2.2) and therefore the IS2 ATL07 geolocated heights
need to be averaged to be spatially congruent with the CS2 footprint. IS2 photons are averaged over 300 m length segments to
165 match the along-track CS2 footprint. Snow depths computed from the IS2 and CS2 height differences were estimated following
Equation (1), and subsequently adjusted with the ocean tidal correction. To identify the extent of spatial heterogeneity in the
retrieved snow depths from Cryo2Ice, the Moran's I test is performed to test the level of spatial autocorrelation. The semi
variogram analysis of the in-situ snow distribution shows that the snow depth values are correlated within a lag distance of ~ 1
kilometer. Therefore, to compare snow distributions representative of each sampled field site (S1 to S4), snow depth is
170 compared over similar roughness zones. Roughness zones corresponding to each Site are defined as a portion of the CS2/IS2
track which had IS2 surface roughness (Section 2.6) within one standard deviation of the IS2 derived surface roughness directly
adjacent to the in-situ sampling site (Figure 1). The Cryo2Ice-derived snow depth corresponding to each roughness site was
then compared against the in-situ snow distribution from the sampling sites.



175 **Figure 3 Methodological workflow for retrieving snow depth (SD) from CS2/IS2 co-registered averaged ATL07 (h (IS2)) and Cryosat-2 heights (h (CS2)) are subtracted following Equation 1. The differenced product is located at the Point of Closest Approach (POCA) of each CS2 footprint. The differenced product is then adjusted with the refractive index (η_s).**

2.6 Adjusting for Sea Surface Height Variation

Assuming IS2 and CS2 are viewing the same landfast ice, any variation in sea surface height over the short 77 minute interval is assumed to be due to tidal variations. The long-period equilibrium tide and ocean-tide with the inverted barometer corrections were compared between the sensors to identify the difference between them. The ocean tide correction, which typically removes the impacts of local tides, had the most significant impact on the height retrievals (Figure C1, See Figure S1 in Bagnardi et al., 2021), with values ranging between +/-50 cm in CS2 and +/-62 cm in IS2 (Kwok et al, 2021, Cryosat-2 Product Handbook). Ideally, the ocean tide correction applied to IS2 and CS2 should account for the variation in SSH due to local tides between passes. Although sea ice has been identified to significantly impact seasonal tidal dampening (Rotermund et al., 2021) it is considered negligible given the short time duration between the passes. Here we compare the average ocean tide corrections to local tidal gauge predictions from the Canadian Hydrographic Service (CHS) (<https://tides.gc.ca>) which are based on real-time and historical tidal gauge measurements from the Cambridge Bay station. The CHS dataset provides instantaneous tidal variations at the CB station every 15 minutes with six observations between the IS2 and CS2 passes. The difference in ocean tidal corrections between the IS2 and CS2 pass was 7.9 cm on average along the track whereas the



difference in water level was 6.0 cm according to the CHS data. The difference in height between IS2 and CS2 was therefore adjusted by a single value of 1.9 cm before the snow depths were computed (Figure 3) and this value then represents a systematic uncertainty on the final snow depth estimates.

2.7 Evaluating Other Sources of Uncertainties

195 One of the critical assumptions is that IS2 and CS2 tracks are roughly coincident i.e. both tracks are measuring roughly the same snow despite their reference ground tracks being ~1.5 km apart. In order to test this assumption Sentinel-1 backscatter (which roughly indicates the snow distribution; Cafarella et al., 2019) was measured across both the IS2 and CS2 reference ground tracks. The SAR pixels intersecting with the IS2 and CS2 track were used to calculate the mean backscatter. The mean difference in backscatter (-0.3 dB) between IS2 (-17.82 dB) and CS2 (-18.11 dB) was less than 1 standard deviation of the backscatter of each track (Figure 4). Since both the tracks have similar backscatter, the assumption that they are coincident and observing snow packs with the same distribution is likely valid.

200

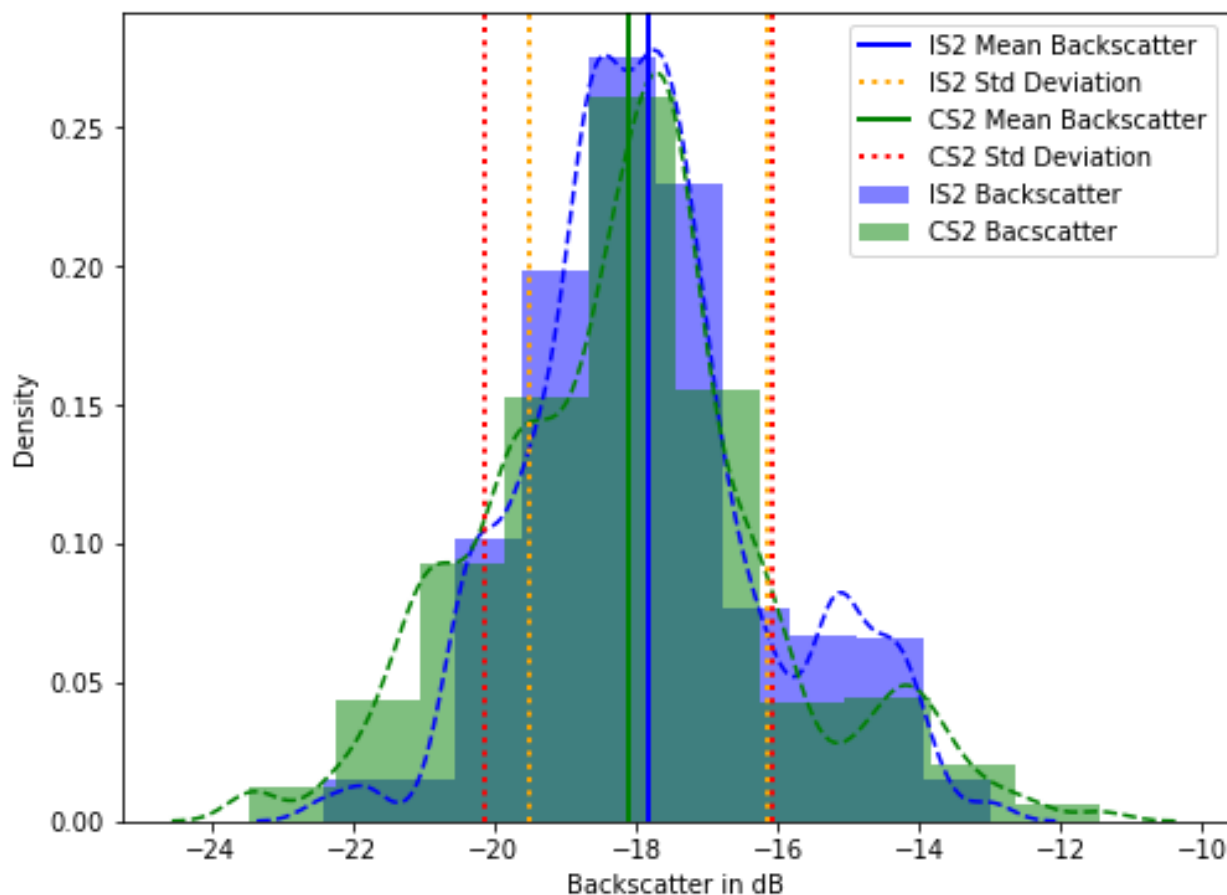


Figure 4 Sentinel-1 Backscatter in dB obtained from the IS2 and CS2 track locations. The Sentinel-1 VH backscatter from 05-05-2022 is used for extracting backscatter along both the tracks in order to assess whether the observed snow distribution is similar.



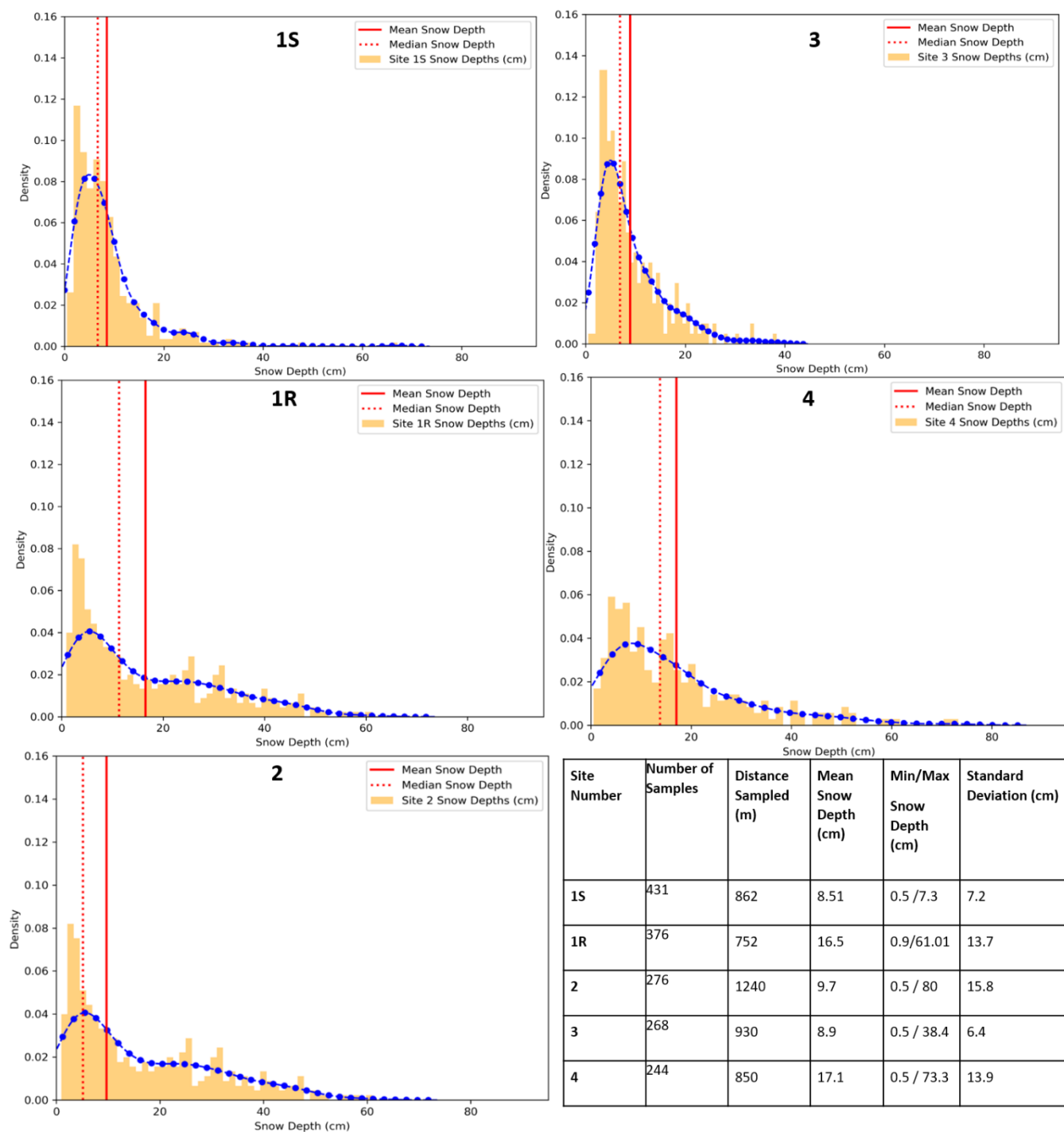
205 Landy et al (2019, 2020) demonstrated the importance of considering surface roughness in the radar data processing. Sea ice surface roughness was computed across the IS2 track using the ATL07 sea ice height product. Following Farrell et al (2020), surface roughness was calculated as the standard deviation of ATL07 sea ice height product calculated over 300-meter length segments to maintain consistency with the spatially averaged ATL07 heights.

Previous studies measured or modelled the dominant scattering surface over first-year sea ice (FYI) at Ku-band several to many centimeters above the snow/sea ice interface even for cold snowpacks. Nandan et al. (2017, 2020) argue that when brine is present within the snowpack, the dominant scattering horizon at Ku-band is shifted by approximately 7 cm above the snow/sea ice interface. Mallett et al., (2020) further demonstrated that the use of fixed snow densities introduced significant biases in the snow depth retrievals. Provided snow salinity impacts the location of the Ku-band dominant scattering horizon (Nandan et al., 2017), an assessment was conducted to test the bias introduced by choosing different snow bulk densities (a) assuming Ku- band microwaves penetrate completely through the snow layers to the sea ice surface and (b) Ku-band microwaves penetrates through layers with snow salinity less than 1 ppt. The corresponding average in-situ snow bulk densities from (a) the complete snow layer (b) snow layers with less than salinity of 1 ppt were used to compute refractive indices followed by respective snow depth calculations. There was negligible difference in the refractive index (<0.05) considering the snow bulk densities with difference in salinity and therefore the average bulk densities from the complete snow pack was used in this study.

3. Results

3.1 In-Situ Snow Depths and Distributions

In-situ snow depths demonstrate significant spatial variability among the four sampled sites (Figure 5). The mean snow depth from the four different sites varies between 9 and 17 cm, and all sites have positively skewed distributions (Figure 5). Site 2 also has some exceptionally high snow depths (> 90 cm), corresponding to the ridged areas (Figure 5) and therefore show higher standard deviations (Figure 5). Sites 2 and 3 have similar snow distributions (Figure 5) but the presence of ridging in Site 2 results in a wider tail compared to Site 3. Site 4 has the highest mean snow depth (Figure 5) as well as the thickest tailed snow distribution (Figure 5).



230 **Figure 5** Snow depth distributions from the four in-situ field measurement sites along the Cryo2Ice transect. The table presents descriptive statistics for the snow depth measurements.

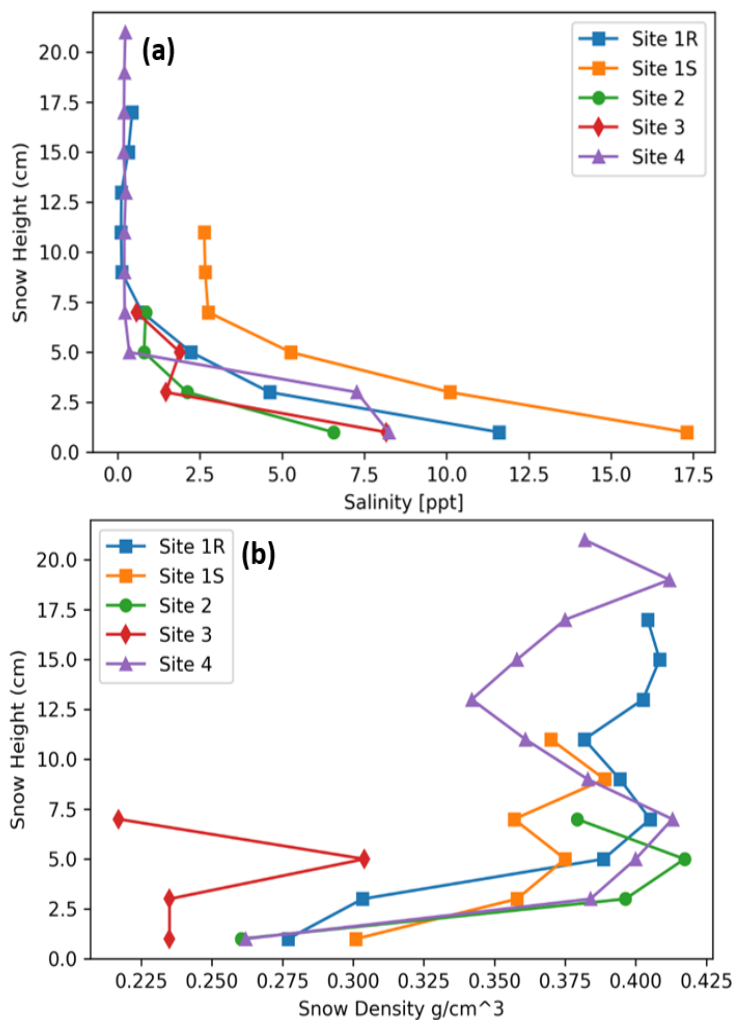


3.2 Snow Geophysical Parameters

Mean snow salinity varies between 1.5 to 3.0 ppt for Sites 1S, 2, 3 and 4, whereas at Site 1S the snow salinity is 6.78 ppt (Figure 6). The mean snow bulk density varies between 0.358 and 0.374 g/cm³ in all sites except Site 3 where the mean snow density is 0.248 g/cm³.
235

Vertical profiles of snow salinity and bulk density present further insights. As shown in Figure 7, the snow density patterns are similar for Sites 1R, 1S, 2 and 4 with bulk density ranging between 0.260 to 0.420 g/cm³ and lower at the base of the snowpack than the surface (Figure 6). The snow density varies in the different snow layers but there is a general trend towards higher densities at 4 to 7 cm above the snow-ice interface at all sites (Figure 6). This is attributed to the presence of a wind slab snow layer most prominent at Sites 1R, 2 and 4.
240

Snow salinity shows higher salinities closer to the snow-ice interface but decreasing with height up the interface (Figure 6 (a)). For snow pits greater than 7.5 cm thick, the salinity is less than 1 ppt closer to the air-snow interface. There is a spike in salinity between 5 to 3 cm from the snow-ice interface at Site 3 that corresponds to the high bulk density snow layer (Figure 6(b)).



Sites	Mean Salinity (ppt)	Mean Bulk Density (g/cm ³)
Site 1R	2.25	0.374
Site 1S	6.78	0.358
Site 2	2.58	0.363
Site 3	3.02	0.248
Site 4	1.59	0.370

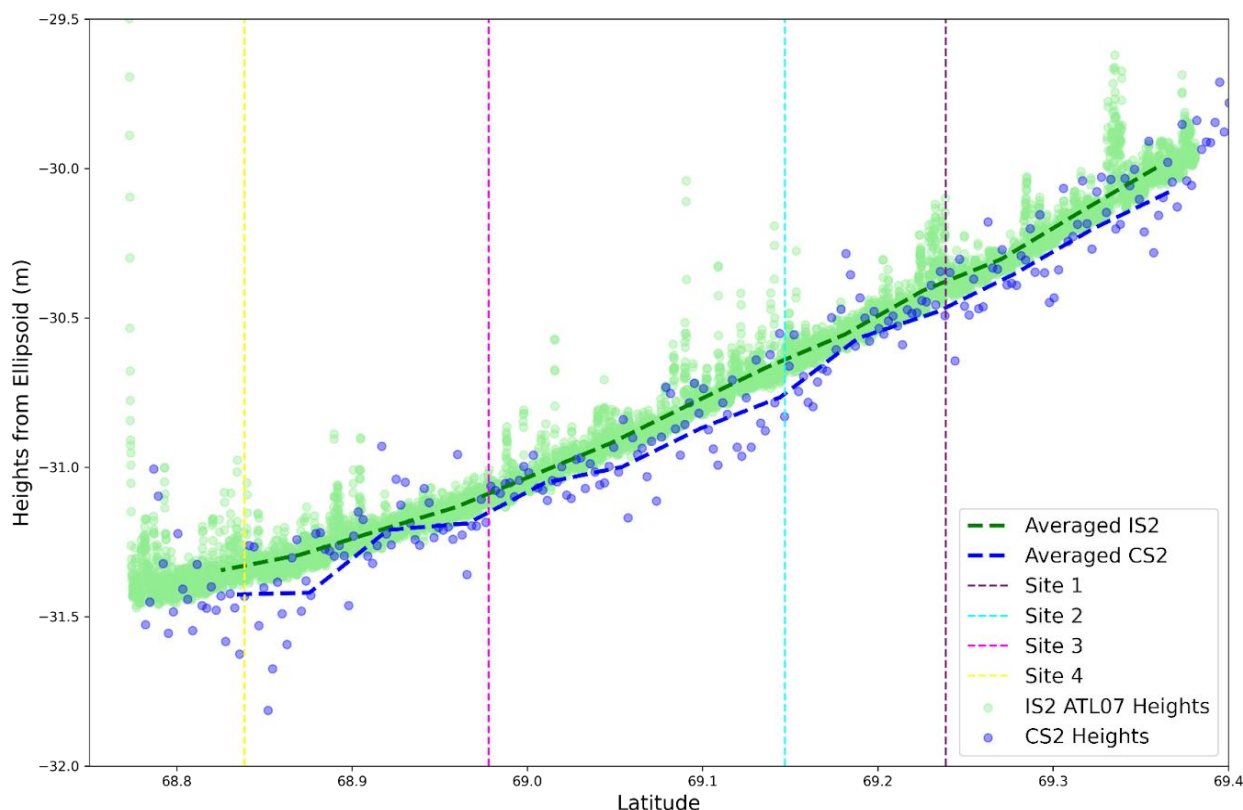
245 **Figure 6 (a) Snow salinity and (b) Snow density change by snow pack depth at the four snow sampling sites. Zero snow depth in both plots represents the snow-ice interface. The bottom table shows the variation in mean salinity and bulk density among the different sites.**

3.3 ICESat-2/Cryosat-2 Derived Snow Depths

The CS2 ($h(CS2)$) and IS2 ($h(IS2)$) heights show a general pattern of lower CS2 heights in comparison to co-registered IS2 heights (Figure 7). The $h(IS2)-h(CS2)$ differences range between -26.5 cm and 50.0 cm with a mean difference of 7.9 cm. 20%

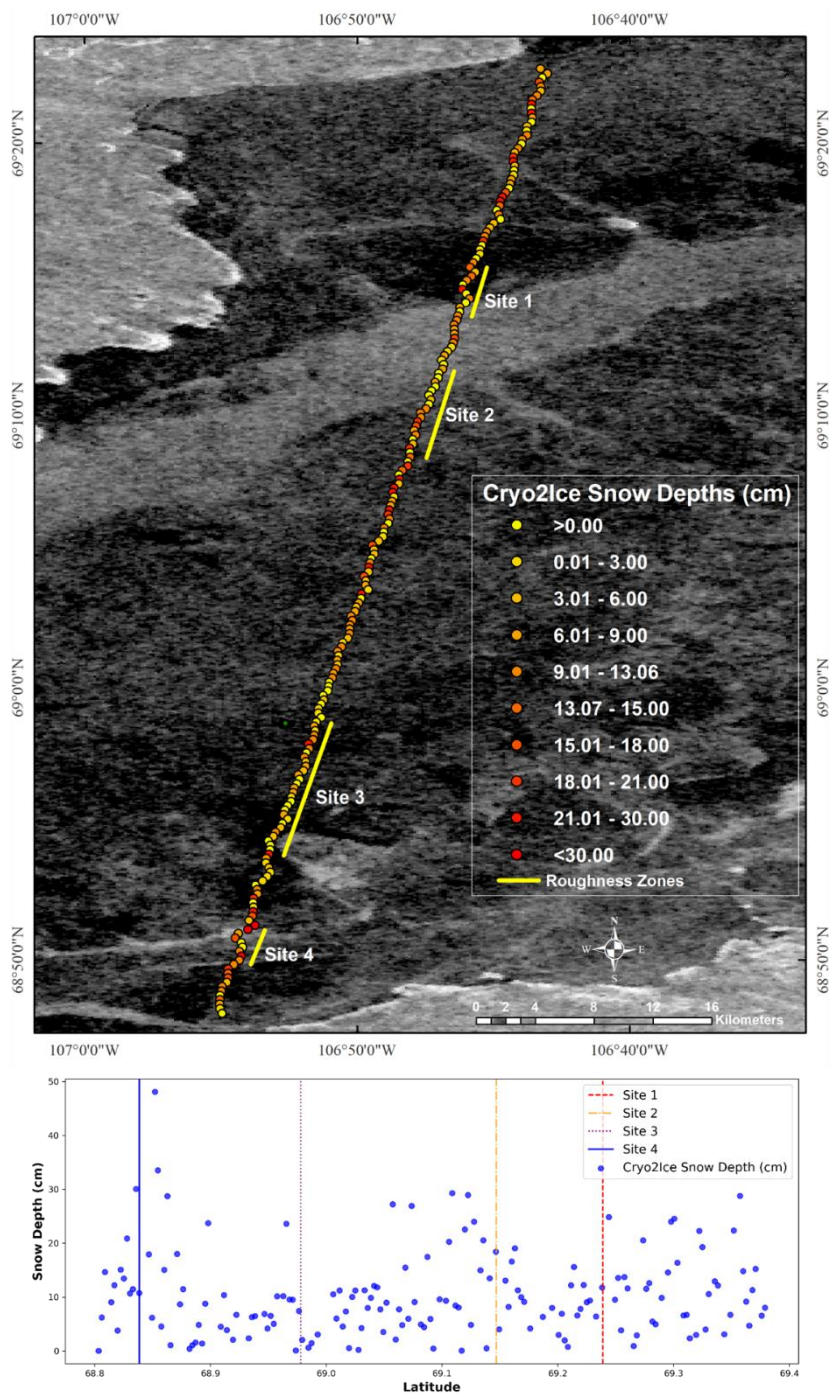


of the calculated differences are negative, with most of them being located closer to the coast i.e., closer to Sites 1 and 4 (Figure 8). The portions of the tracks having negative differences are excluded from the subsequent calculation of snow depths. The adjusted mean snow depth across the whole Cryo2Ice track is 10.4 cm, marginally lower than the in-situ mean snow depth of 11.9 cm (Figure 5). Snow depths shown in Figure 9(b) display a right-skewed distribution with a sharper and heavier tail compared to a normal distribution. This is consistent with the distributions obtained from the in-situ snow sites (Figure 5). A maximum snow depth of 48.1 cm is retrieved from Cryo2Ice, at a length scale of 300 m.



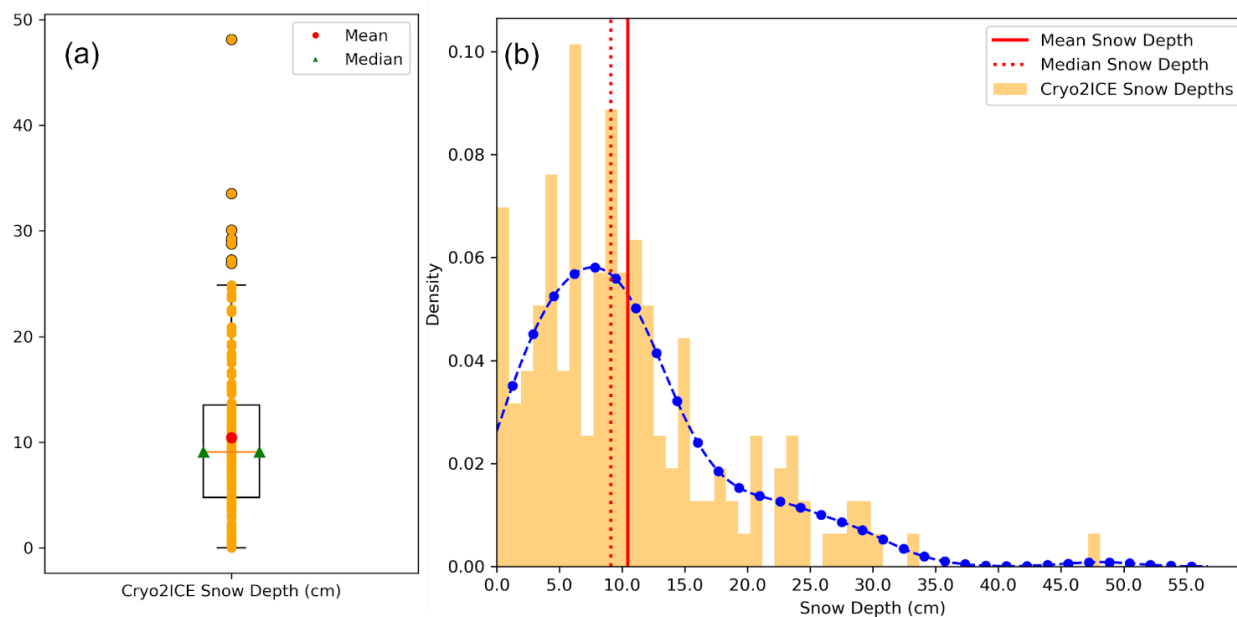
260 **Figure 7 IS2 ATL07 sea ice heights plotted along with CS2 surface heights. Note, the reported heights are relative heights and can be negative because of the WGS84 ellipsoid reference heights in the study area. The green and blue dashed lines indicate averaged heights over 5 km along-track distances.**

The semivariogram analysis indicates that there is spatial autocorrelation among measured snow depths within ~1 km but there is no significant autocorrelation for larger distances, along this specific track. This also implies that there is significant spatial heterogeneity above the km-scale along the ~65 km track (Figure 8). The snow depths are correlated at scales under ~1 km which correspond with the lengths of the representative portions of the track delineated with similar roughness (Figure 8).



265

Figure 8 Spatial distribution of 300-m scale snow depths across the CS2 and IS2 derived track. The background image is a Sentinel-1 HH backscatter image from 5-05-2022. The bottom plot shows the along-track Cryo2Ice snow depth variation plotted against latitude.



270 **Figure 9 (a) Boxplot showing the distribution of Cryo2Ice snow depth along with the mean and median snow depths symbolized (b) Histogram showing the density distribution of the retrieved snow depth along the Cryo2Ice track with the mean and the median snow depths.**

4 Discussion

4.1 Comparison with Past Studies

275 Previous field observations from Yackel et al. (2019) and Nandan et al. (2020) suggest that mean snow depth on FYI in Dease Strait during late winter ranges between 10 and 30 cm depth (Table 1). Both our mean in-situ snow depth measurements (11.9 cm) and Cryo2Ice retrieved mean snow depths (10.4 cm), are within the typical range reported in previous surveys (Table 1).

280

285



Table 1 In-situ snow depth measurements at Dease Strait. The range of mean snow depths represents the range of mean snow depths retrieved from the sampled sites.

290

Sampling Period	Mean Snow Depth (cm)	Number of Sites Sampled	Total Number of Samples	Sampling Technique	Reference
20 April to 9 June, 2014	13.5	24	24	Snow Pits	Campbell et al., (2016)
12 May to 17 June, 2014	20.8	2	60	Meter Rule Sampling	Diaz et al., (2014)
19-22 April, 2014	12.0/18.0	20	5200	Meter Rule Sampling	Zheng et al., (2017)
23-26 May, 2016	12.0/22.0	4	2100	Meter Rule Sampling	Moon et al., (2019)
01-08 April, 2017	17.0/ 35.0	5	2161	Magnaprobe Sampling	Moon et al., (2019)
17-19 May, 2018	20.9 / 21.8	3		Magnaprobe Sampling	Yackel et al., (2019)
1 May, 2022	11.9	4	1596	Magnaprobe Sampling	This Study
Cryo2Ice Snow Depths	10.4 (Mean), 48.1 (Maximum)				

4.2 Snow Depth: Cryo2Ice vs In-situ

Cryo2Ice snow depths showed similar relative patterns when compared to in-situ snow depth sampling. The thinnest (Site 3) and thickest (Site 4) mean snow depths found in the in-situ measurements are corroborated with Cryo2Ice snow depths as well (Table 2). The Kruskal-Wallis non-parametric test was conducted to assess statistically significant differences between the



snow depths retrieved from the in-situ and Cryo2Ice. The test results show significant difference between in-situ sites which was also evident in the corresponding Cryo2Ice snow depths.

Although the mean snow depth for the entire studied Cryo2Ice track was 10.4 cm, the mean snow depth from Cryo2Ice samples at the site locations was 9.9 cm. This compares to a mean in-situ snow depth of 11.9 cm (Table 2). Cryo2Ice snow depths are on average 2.15 cm thinner than the in-situ data, which is a 0.5 cm larger difference than the manual tidal correction we applied to compare the CS2 and IS2 track heights (i.e., the largest known systematic uncertainty during processing). This pattern of a few cm mean snow depth underestimations by Cryo2Ice is consistently observed across three of the four sites: Sites 1, 2 and 3 (Figure 10).

305 **Table 2 In-situ versus Cryo2Ice snow distribution statistics**

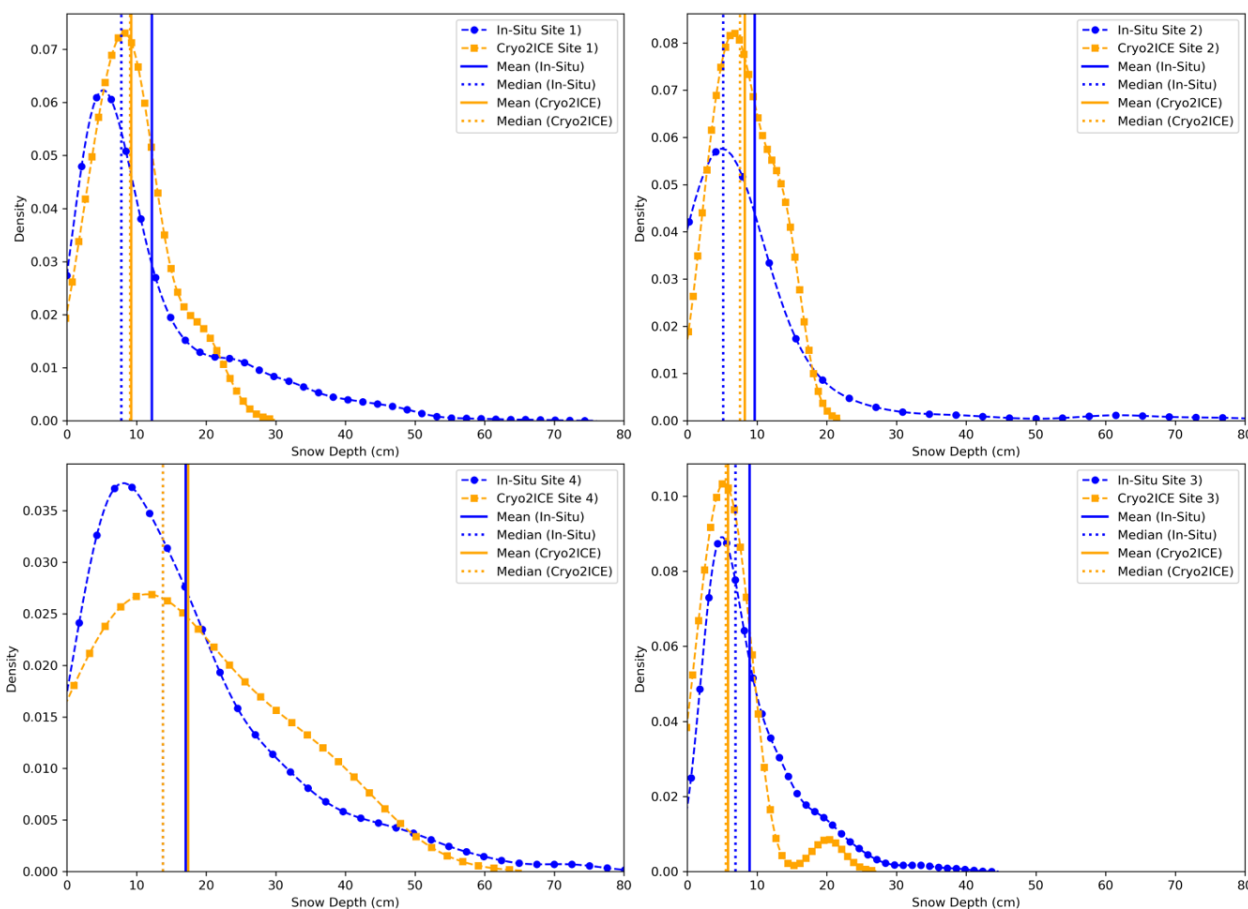
		Mean (cm)	Median (cm)	Lower (cm)	Quartile	Upper (cm)	Quartile	Inter-quartile (cm)	range
Site 1	In-Situ	12.2	7.8	4.1		16.3		12.2	
	Cryo2Ice	8.9	8.8	5.8		10.2		4.4	
Site 2	In-Situ	9.7	5.2	3.7		9.2		5.5	
	Cryo2Ice	8.1	7.4	5.2		11.1		5.9	
Site 3	In-Situ	8.9	6.9	4.2		11.9		7.7	
	Cryo2Ice	5.4	5.2	3.1		7.7		4.6	
Site 4	In-Situ	17.1	13.8	6.7		22.4		15.7	
	Cryo2Ice	17.1	13.5	7.9		22.9		15.0	

While the mean snow depth seems to be highly impacted by the presence of high snow depth sites especially around ridges, the median snow depth presents a more representative statistic for comparing the retrieved Cryo2Ice snow depth with the in-situ distribution. The median snow depths retrieved from Cryo2Ice are accurate to within ± 2.0 cm of median snow depths retrieved from all the different sites. There was an overestimation of the median snow depth by 1.0 cm and 2.2 cm for Sites 1 and Site 2 respectively while there was an overestimation of snow depths at Site 3 (1.7 cm). The best correspondence between the Cryo2Ice distributions in terms of median snow depth can be found in Site 4 which had a median snow depth much higher than the rest of the sites (Table 4).

We also notice that the impact of ridging on the overall accuracy of the technique was significant. The standard deviation of the in-situ snow depths is highest (Figure 5) and ridging is picked up from IS2 heights (Figure 7) at Site 2 where Cryo2Ice performs the worst. In terms of the overall shape of the distributions, the best match is found for Site 3 which has the lowest median snow depth among the sites. These mismatches may be caused by the difference in sampling length-scales between



320 Cryo2Ice, which is at the kilometer scale, compared to in-situ measurements which are retrieved over 100s of meters. It is evident that while IS2 has a much finer resolution, the larger footprint of CS2 means that the spatial variability of snow depths under the kilometer scale are not well represented by Cryo2Ice. For instance, the Cryo2Ice snow depths are consistently truncated at the thick end of the distribution, with at least some portion of the in-situ distributions above ~30-50 cm seemingly unresolved from space (Figure 10).



325 **Figure 10 Probability Density plots comparing In-Situ snow depths to Cryo2Ice retrieved snow depths along with the median and mean values.**

4.3 Snow Geophysical Properties and Cryo2Ice Retrievals

Both snow salinity and bulk density changes across the snowpack layer impacts the IS2 laser and CS2 radar waveform interactions with the snowpack. While the IS2 green laser is mostly impacted by the air-snow interface conditions, CS2 radar waveforms interact with different layers of the snowpack and the dominant scattering horizon and subsequently radar heights can potentially be impacted by the snow properties. There were significant differences among the snow salinity and density

330



characteristics (Figure 6) between the surveyed sites. We notice that Cryo2Ice performs best in Site 4 which has the lowest mean snow salinity and has non-saline (<1 ppt) snow layers for the largest portion of the snow pack (Figure 6). Therefore, with 17 cm out of the 22 cm deep snowpack at Site 4 being non-saline, the maximum intensity of the CS2 backscatter may have been sourced from closer to the sea-ice interface. On the contrary, highly saline layers can potentially raise the height of dominant scattering intensity of the Ku-band radar leading to overestimated CS2 heights ($h(CS2)$) and subsequently lower mean snow depth compared to in-situ values. This phenomenon of snow depth underestimation was evident in Sites 1R, 1S and 2 potentially because of the sharp increase in snow salinity within the first 5 cm (from the air-snow interface) of the snowpack (Figure 6) and may have contributed to the 2-3 cm mean underestimation of Cryo2Ice snow depths.

The impact of snow bulk density on the Cryo2Ice retrievals was less likely except for the presence of wind-slab layers which are identified as stark increases in snow bulk densities within the snow pack. The wind-slab layers identified in Sites 1R, 2 and 4 reach to 0.425 g/cm^3 compared to 0.358 to 0.374 g/cm^3 on average throughout the snow pack which may have caused hindrance to Ku-band penetration. The presence of this high-density snow layer along with the reduction in Ku-band speed due to power attenuation of Ku-band microwaves may potentially cause a cumulative upward shift of the dominant scattering horizon resulting in underestimation of snow depths.

345 **4.4 Sea Surface Height Estimation and Cryo2Ice Retrievals**

Canadian Hydrographic Service (CHS) tidal predictions for 29 April 2022 suggest the satellite overpasses occurred during a low tide period. According to the predictions, the water level was 6 cm higher for the IS2 pass at 21:18 UTC than for the CS2 pass at 22:35 UTC (Appendix 3). This 6 cm water level difference should ideally be accounted for by the difference in IS2 and CS2 ocean tide corrections. The IS2 ATL07 heights were reduced by a mean ocean tide correction of -0.71 cm whereas the CS2 Heights reduced by an average ocean tide correction of -8.64 cm. Therefore, the difference between IS2 heights and CS2 heights was increased by 7.9 cm due to the ocean tide correction adjustment but the CHS predictions suggest it should have been only 6.0 cm. This 1.9 cm difference would introduce a 17% bias in retrieved snow depths, given the approx. mean snow depths we measured in-situ. This error could be attributed to the ocean tide corrections used in IS2 and CS2 originating from two different models i.e. GOT 4.8 (IS2) and FES 2004 (CS2). To put this source of error into wider context, past CS2 and IS2 coincident tracks from 15-04-2021 and 14-05-2021 were also analysed. We found a bias of 2 to 5 cm when compared with the CHS dataset, meaning that we can expect ~15-40% systematic uncertainty in Cryo2Ice retrieved snow depths owing to the uncertainty in tidal differences between satellite passes. This is a significant uncertainty, but it is systematic and varies at the length-scale of the tidal corrections (100s km), so it will not affect the *relative* variations in retrieved snow depth along track, only their *absolute* magnitude. Therefore, Cryo2Ice seems capable of measuring the relative variations in snow depth between different locations of the CAA without the availability of sea surface reference tie-points.



4.5 Surface Roughness and Cryo2Ice retrievals

Surface roughness calculated from IS2 was used to analyze the Cryo2Ice snow depths between sites with different roughness. There was only a weak positive correlation (R^2 0.04) between surface roughness retrieved from IS2 and Cryo2Ice snow depths. Site 4 had the highest mean surface roughness (4.58 cm) whereas the other sites had roughness ranging between 2.4-2.7 cm. Although there was significant ridging in Site 2 and IS2 does pick up some of the ridges (Figure 7), the mean surface roughness is low (2.48 cm) because of the extensive areas of thin snow cover which dominates the laser returns. While Site 4 had the highest snow depth as well as highest surface roughness from IS2, the Cryo2Ice retrievals were most accurate both in terms of mean and median bias among all the four sites (Figure 11). However, one stark difference was the fact that there was no ridging in Site 4. Therefore, while there were extensive areas of rough sea ice with snow depths between 20 and 50 cm, there were hardly any snow depths greater than 80 cm (Figure 10). We also notice that for Site 2, the majority of the snow was very thin with only a few very high snow depth points especially around the ridges (Figure 10). The presence of isolated ridges and the deeper snow accumulated around them may have been missed by the CryoSat-2 radar given the larger impact of level ice versus ridges on the backscattered power. The ridge heights may also be underestimated with current ICESat-2 processing methods (Ricker et al., 2023) meaning that snow depths would be underestimated. The higher variability which is indicated by the standard deviation of snow depths translates to greater mean bias in snow depth (Figure 5).

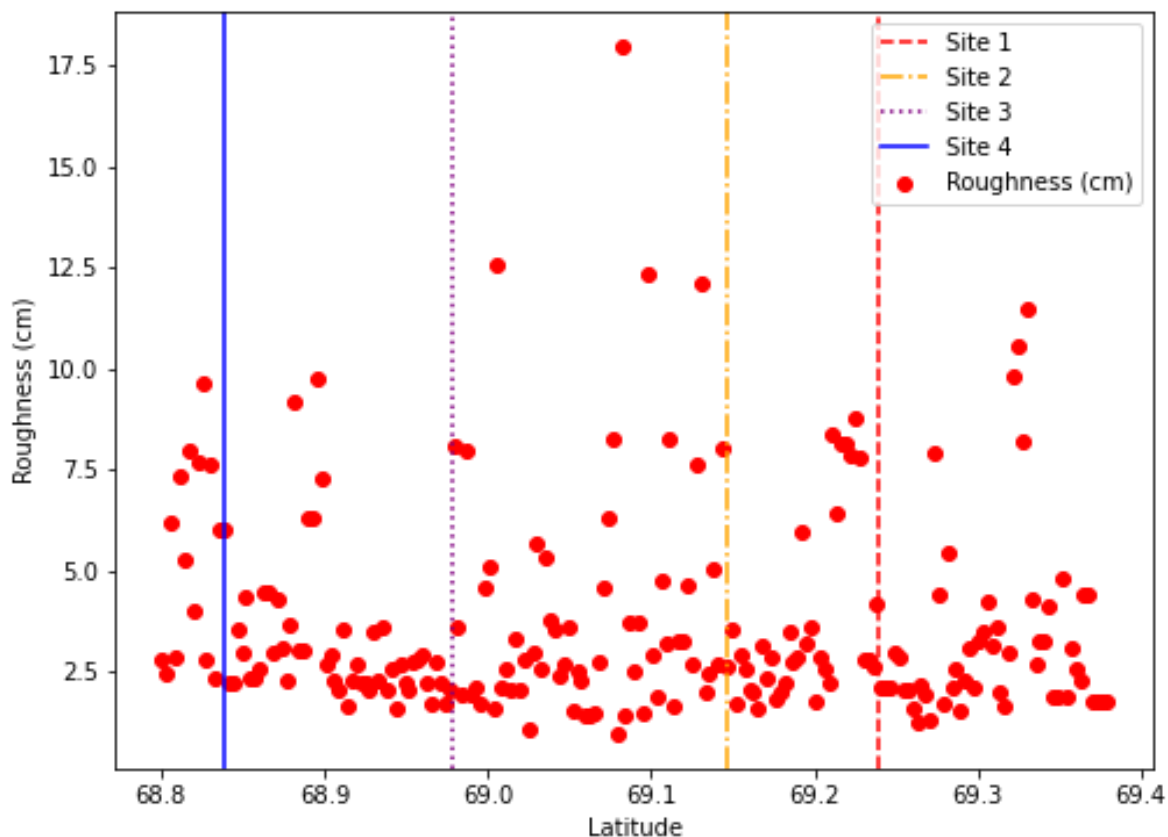


Figure 11 Variation in surface roughness along the Cryo2Ice track at the four in-situ snow thickness validation sites

5 Conclusion

380 Accurate snow depth monitoring over landfast ice in the Canadian Arctic Archipelago (CAA) is important for communities that rely on landfast ice for transportation and their livelihood (Mahoney et al., 2009). It is imperative to monitor snow depth in the CAA as there have been reports of declining snow depths at a rate of 0.8 cm per decade in Cambridge Bay and at other locations in the CAA (Howell et al., 2016; Lam et al., 2023). Moreover, they reported snow depth on sea ice trends were highly correlated to the declining sea ice thickness. Therefore, this study explores the potential of retrieving snow depth using
385 Cryo2Ice in a lead-less regions of the Canadian Arctic Archipelago.

Snow depth from Cryo2Ice is retrieved based on the elevation difference between IS2 and CS2 sea ice heights from a common ellipsoid as opposed to the popular freeboard differencing method. The instantaneous difference in sea level between the ~1.5hour difference between the CS2 and IS2 passes is accounted for by adjusting the ocean tide corrections with local tide model predictions. The snow depths retrieved from Cryo2Ice compare favourably with in-situ snow depth measurements. The
390 relative snow depth patterns from in-situ field sites were corroborated with Cryo2Ice measurements, i.e. the thinnest and



thickest snow depth regions were picked up correctly by Cryo2Ice. The mean snow depth from Cryo2Ice of 10.4 cm is realistic compared to in-situ measurements from this study and previous studies conducted at the Dease Strait. The site-wise comparison between in-situ snow depths and Cryo2Ice snow depths from representative roughness zones demonstrates that the best correspondence is from sites which have the thickest snow and fewest ridges. Differences in the shapes of the distributions from in-situ sites and representative roughness zones of the Cryo2Ice are mostly a result of the difference in sampling resolutions of Cryo2Ice (~300 m) and the in-situ measurements (5 m). The tails of the in-situ snow depth distributions (> 40 cm) were largely missed by Cryo2Ice and the Cryo2Ice snow depth retrieval accuracy is impacted by the presence of sea ice ridges, with ridged sites having underestimated snow depths by as much as ~ 3.3 cm.

Snow geophysical properties especially snow salinity in the deepest few centimeters of the snow pack, may impact the dominant scattering centre of the CS2 radar return and can lead to underestimation of the snow depths. The snow depth was slightly underestimated in 3 out of 4 sites by 20.7% compared to in-situ measurements. However, median Cryo2Ice snow depths – reducing the impact of the missing thick snow tail in Cryo2Ice snow depth distributions – did not generally underestimate the in-situ values. Therefore, such physical factors (ridging, high salinity) did not seem to produce biases greater than the systematic uncertainty on the difference in ocean tidal corrections (1.90 cm), for our studied track. If these physical biases were larger for another scenario/track, when the tidal uncertainty is zero (i.e., in areas with leads) or snow pack thicker/roughness larger, they may have significant impacts on the retrieval process. However, it is difficult to attribute a few centimeters of bias to snow geophysical process, surface roughness and/or errors in the altimeters' tidal corrections. Therefore, further studies are required in different lead-less regions under varying snow conditions for improved insights into the sources of bias in snow depth retrievals from Cryo2Ice. Findings from this study are encouraging for estimating snow depth on land-fast sea ice in lead-less regions using Cryo2Ice and for future coincident laser-radar or dual-frequency altimeter missions.

Data Availability

ICESat-2 ATL07 data may be accessed from the NSIDC website (See: <https://nsidc.org/data/atl07q1/versions/6#anchor-2>). Cryosat-2 data may be accessed from ESA (<https://eocat.esa.int/>). The snow depth validation dataset maybe made available upon request.

Author Contribution

MS, JS and DI were involved in the conceptualization of the study. MS, JS, JY, HML and VN were involved in planning of the field campaign. JS acquired the funding for the research. MS, JY and HML collected the snow and sea ice physical property validation data from the field. MS, JS, DI, JL and VN were involved were involved in formulating the methodology for the analysis. MS prepared the original draft. All co-authors were involved in the review and editing process.

420



Competing Interests

At least one of the (co-)authors is a member of the editorial board of The Cryosphere.

Acknowledgements

425 The authors would like to acknowledge Torsten Geldsetzer from the University of Calgary for his input during the planning stages of the Cambridge Bay campaign. We acknowledge Nathan Kurtz from NASA for providing early ICESat-2 ATL07 release 006 data which was vital for the analysis. MS was supported by ArcticNet (Grant Number #52551), Julienne Stroeve's NSERC Canada 150 Chair (Grant Number #50297) and University of Manitoba Graduate Student Fellowship (UMGF). We also acknowledge support from ArcticNet Field Aircraft Support for the helicopter support.

430 References

- Andersen, O. B., Nilsen, K., Sørensen, L. S., Skourup, H., Andersen, N. H., Nagler, T., Wuite, J., Kouraev, A., Zakharova, E., and Fernandez, D.: Arctic freshwater fluxes from earth observation data: International Review Workshop on Satellite Altimetry Cal/Val Activities and Applications, Fiducial Reference Measurements for Altimetry, 97–103, https://doi.org/10.1007/1345_2019_75, 2019.
- 435 Andreas, E. L., Jordan, R. E., and Makshtas, A. P.: Parameterizing turbulent exchange over sea ice: the ice station weddell results, *Boundary-Layer Meteorology*, 114, 439–460, <https://doi.org/10.1007/s10546-004-1414-7>, 2005.
- Bagnardi, M., Kurtz, N. T., Petty, A. A., and Kwok, R.: Sea Surface Height Anomalies of the Arctic Ocean From ICESat-2: A First Examination and Comparisons With CryoSat-2, *Geophys. Res. Lett.*, 48, e2021GL093155, <https://doi.org/10.1029/2021GL093155>, 2021.
- 440 Beaven, S. G., Lockhart, G. L., Gogineni, S. P., Hossetnmostafa, A. R., Jezek, K., Gow, A. J., Perovich, D. K., Fung, A. K., And Tjuatja, S.: Laboratory measurements of radar backscatter from bare and snow-covered saline ice sheets, *International Journal of Remote Sensing*, 16, 851–876, <https://doi.org/10.1080/01431169508954448>, 1995.
- Blanchard-Wrigglesworth, E., Webster, M. A., Farrell, S. L., and Bitz, C. M.: Reconstruction of Snow on Arctic Sea Ice, *Journal of Geophysical Research: Oceans*, 123, 3588–3602, <https://doi.org/10.1002/2017JC013364>, 2018.
- 445 Brunt, K. M., Neumann, T. A., and Smith, B. E.: Assessment of ICESat-2 Ice Sheet Surface Heights, Based on Comparisons Over the Interior of the Antarctic Ice Sheet, *Geophysical Research Letters*, 46, 13072–13078, <https://doi.org/10.1029/2019GL084886>, 2019.
- Cafarella, S. M., Scharien, R., Geldsetzer, T., Howell, S., Haas, C., Segal, R., and Nasonova, S.: Estimation of Level and Deformed First-Year Sea Ice Surface Roughness in the Canadian Arctic Archipelago from C- and L-Band Synthetic Aperture Radar, *Can. J. Remote Sens.*, 45, 457–475, <https://doi.org/10.1080/07038992.2019.1647102>, 2019.
- 450



- Campbell, K., Mundy, C. J., Landy, J. C., Delaforge, A., Michel, C., and Rysgaard, S.: Community dynamics of bottom-ice algae in Dease Strait of the Canadian Arctic, *Prog. Oceanogr.*, 149, 27–39, <https://doi.org/10.1016/j.pocean.2016.10.005>, 2016.
- De Rijke-Thomas, C., Landy, J. C., Mallett, R., Willatt, R. C., Tsamados, M., and King, J.: Airborne Investigation of Quasi-Specular Ku-Band Radar Scattering for Satellite Altimetry Over Snow-Covered Arctic Sea Ice, *IEEE Trans. Geosci. Remote Sens.*, 61, 1–19, <https://doi.org/10.1109/TGRS.2023.3318263>, 2023.
- 455 Diaz, A., Ehn, J. K., Landy, J. C., Else, B. G. T., Campbell, K., and Papakyriakou, T. N.: The Energetics of Extensive Meltwater Flooding of Level Arctic Sea Ice, *J. Geophys. Res. Oceans*, 123, 8730–8748, <https://doi.org/10.1029/2018JC014045>, 2018.
- Eicken, H., Grenfell, T. C., Perovich, D. K., Richter-Menge, J. A., and Frey, K.: Hydraulic controls of summer Arctic pack ice albedo, *Journal of Geophysical Research: Oceans*, 109, <https://doi.org/10.1029/2003JC001989>, 2004.
- 460 ESA: CryoSat-2 Product Handbook, 2013.
- ESA: About CRYO2ICE - Earth Online:<https://earth.esa.int/eogateway/missions/cryosat/cryo2ice>, last access: 20 October 2023, 2020.
- Farrell, S., Duncan, K., Yi, D., Hendricks, S., Ricker, R., Buckley, E., and Baney, O.: Optimizing Dual-Band Satellite Altimetry to Map Declining Arctic Sea Ice, 2021, C31B-05, 2021.
- 465 Fons, S. W., Kurtz, N. T., Bagnardi, M., Petty, A. A., and Tilling, R. L.: Assessing CryoSat-2 Antarctic Snow Freeboard Retrievals Using Data From ICESat-2, *Earth Space Sci.*, 8, e2021EA001728, <https://doi.org/10.1029/2021EA001728>, 2021.
- Galley, R. J., Else, B. G. T., Howell, S. E. L., Lukovich, J. V., And Barber, D. G.: Landfast Sea Ice Conditions in the Canadian Arctic: 1983-2009, *Arctic*, 65, 133–144, 2012.
- Howell, S. E. L., Laliberté, F., Kwok, R., Derksen, C., and King, J.: Landfast ice thickness in the Canadian Arctic Archipelago from observations and models, *The Cryosphere*, 10, 1463–1475, <https://doi.org/10.5194/tc-10-1463-2016>, 2016.
- 470 Kacimi, S. and Kwok, R.: The Antarctic sea ice cover from ICESat-2 and CryoSat-2: freeboard, snow depth, and ice thickness, *The Cryosphere*, 14, 4453–4474, <https://doi.org/10.5194/tc-14-4453-2020>, 2020.
- Kern, S., Khvorostovsky, K., Skourup, H., Rinne, E., Parsakhoo, Z. S., Djepa, V., Wadhams, P., and Sandven, S.: The impact of snow depth, snow density and ice density on sea ice thickness retrieval from satellite radar altimetry: results from the ESA-CCI Sea Ice ECV Project Round Robin Exercise, *The Cryosphere*, 9, 37–52, <https://doi.org/10.5194/tc-9-37-2015>, 2015.
- 475 Kurtz, N. T. and Farrell, S. L.: Large-scale surveys of snow depth on Arctic sea ice from Operation IceBridge, *Geophysical Research Letters*, 38, <https://doi.org/10.1029/2011GL049216>, 2011.
- Kwok, R. and Markus, T.: Potential basin-scale estimates of Arctic snow depth with sea ice freeboards from CryoSat-2 and ICESat-2: An exploratory analysis, *Advances in Space Research*, 62, 1243–1250, <https://doi.org/10.1016/j.asr.2017.09.007>, 2018.
- 480 Kwok, R., Cunningham, G., Hancock, D., Ivanoff, A., and Wimert, J.: Algorithm Theoretical Basis Document (ATBD) For Sea Ice Products, 2018.



- Kwok, R., Kacimi, S., Markus, T., Kurtz, N. T., Studinger, M., Sonntag, J. G., Manizade, S. S., Boisvert, L. N., and Harbeck, J. P.: ICESat-2 Surface Height and Sea Ice Freeboard Assessed With ATM Lidar Acquisitions From Operation IceBridge, *Geophysical Research Letters*, 46, 11228–11236, <https://doi.org/10.1029/2019GL084976>, 2019.
- 485 Kwok, R., Bagnardi, M., Petty, A., and Kurtz, N.: ICESat-2 sea ice ancillary data - Mean Sea Surface Height Grids, <https://doi.org/10.5281/zenodo.4294048>, 2020.
- Kwok, R., Petty, A. A., Bagnardi, M., Kurtz, N. T., Cunningham, G. F., Ivanoff, A., and Kacimi, S.: Refining the sea surface identification approach for determining freeboards in the ICESat-2 sea ice products, *The Cryosphere*, 15, 821–833, <https://doi.org/10.5194/tc-15-821-2021>, 2021.
- 490 Kwok, R., Petty, A., Bagnardi, M., Wimert, J. T., Cunningham, G. F., Hancock, D. W., Ivanoff, A., and Kurtz, N.: Ice, Cloud, and Land Elevation Satellite (ICESat-2) Project Algorithm Theoretical Basis Document (ATBD) for Sea Ice Products, version 6, <https://doi.org/10.5067/9VT7NJWOTV3I>, 2023.
- Lam, H.-M., Geldsetzer, T., Howell, S.E.L., and Yackel, J. Snow Depth on Sea Ice and on Land in the Canadian Arctic from *Long-Term Observations, Atmosphere-Ocean*, 61:4, 217-233, <https://doi.org/10.1080/07055900.2022.2060178>, 2023.
- 495 Landy, J. C., Petty, A. A., Tsamados, M., and Stroeve, J. C.: Sea Ice Roughness Overlooked as a Key Source of Uncertainty in CryoSat-2 Ice Freeboard Retrievals, *Journal of Geophysical Research: Oceans*, 125, e2019JC015820, <https://doi.org/10.1029/2019JC015820>, 2020.
- Laxon, S. W., Giles, K. A., Ridout, A. L., Wingham, D. J., Willatt, R., Cullen, R., Kwok, R., Schweiger, A., Zhang, J., Haas, C., Hendricks, S., Krishfield, R., Kurtz, N., Farrell, S., and Davidson, M.: CryoSat-2 estimates of Arctic sea ice thickness and volume, *Geophysical Research Letters*, 40, 732–737, <https://doi.org/10.1002/grl.50193>, 2013.
- 500 Leuschen, C. J., Swift, R. N., Comiso, J. C., Raney, R. K., Chapman, R. D., Krabill, W. B., and Sonntag, J. G.: Combination of laser and radar altimeter height measurements to estimate snow depth during the 2004 Antarctic AMSR-E Sea Ice field campaign, *Journal of Geophysical Research: Oceans*, 113, <https://doi.org/10.1029/2007JC004285>, 2008.
- 505 Magruder, L. A., Brunt, K. M., and Alonzo, M.: Early ICESat-2 on-orbit Geolocation Validation Using Ground-Based Corner Cube Retro-Reflectors, *Remote Sensing*, 12, 3653, <https://doi.org/10.3390/rs12213653>, 2020.
- Mahoney, A., Gearheard, S., Oshima, T., and Qillaq, T.: Sea Ice Thickness Measurements from a Community-Based Observing Network, *Bulletin of the American Meteorological Society*, 90, 370–378, <https://doi.org/10.1175/2008BAMS2696.1>, 2009.
- 510 Maykut, G. A. and Untersteiner, N.: Some results from a time-dependent thermodynamic model of sea ice, *Journal of Geophysical Research (1896-1977)*, 76, 1550–1575, <https://doi.org/10.1029/JC076i006p01550>, 1971.
- Meier, W. and Stroeve, J.: An Updated Assessment of the Changing Arctic Sea Ice Cover, *Oceanog*, <https://doi.org/10.5670/oceanog.2022.114>, 2022.
- Melling, H.: Sea ice of the northern Canadian Arctic Archipelago, *Journal of Geophysical Research: Oceans*, 107, 2-1-2–21, <https://doi.org/10.1029/2001JC001102>, 2002.
- 515



- Mundy, C. J., Barber, D. G., and Michel, C.: Variability of snow and ice thermal, physical and optical properties pertinent to sea ice algae biomass during spring, *Journal of Marine Systems*, 58, 107–120, <https://doi.org/10.1016/j.jmarsys.2005.07.003>, 2005.
- Moon, W., Nandan, V., Scharien, R. K., Wilkinson, J., Yackel, J. J., Barrett, A., Lawrence, I., Segal, R. A., Stroeve, J., 520 Mahmud, M., Duke, P. J., and Else, B.: Physical length scales of wind-blown snow redistribution and accumulation on relatively smooth Arctic first-year sea ice, *Environ. Res. Lett.*, 14, 104003, <https://doi.org/10.1088/1748-9326/ab3b8d>, 2019.
- Nandan, V., Geldsetzer, T., Yackel, J., Mahmud, M., Scharien, R., Howell, S., King, J., Ricker, R., and Else, B.: Effect of Snow Salinity on CryoSat-2 Arctic First-Year Sea Ice Freeboard Measurements, *Geophysical Research Letters*, 44, 10,419–10,426, <https://doi.org/10.1002/2017GL074506>, 2017.
- 525 Nandan, V., Scharien, R. K., Geldsetzer, T., Kwok, R., Yackel, J. J., Mahmud, M. S., Rösel, A., Tonboe, R., Granskog, M., Willatt, R., Stroeve, J., Nomura, D., and Frey, M.: Snow Property Controls on Modeled Ku-Band Altimeter Estimates of First-Year Sea Ice Thickness: Case Studies From the Canadian and Norwegian Arctic, *IEEE Journal of Selected Topics in Applied Earth Observations and Remote Sensing*, 13, 1082–1096, <https://doi.org/10.1109/JSTARS.2020.2966432>, 2020.
- Neumann, T. A., Martino, A. J., Markus, T., Bae, S., Bock, M. R., Brenner, A. C., Brunt, K. M., Cavanaugh, J., Fernandes, S. 530 T., Hancock, D. W., Harbeck, K., Lee, J., Kurtz, N. T., Luers, P. J., Luthcke, S. B., Magruder, L., Pennington, T. A., Ramos-Izquierdo, L., Rebold, T., Skoog, J., and Thomas, T. C.: The Ice, Cloud, and Land Elevation Satellite – 2 mission: A global geolocated photon product derived from the Advanced Topographic Laser Altimeter System, *Remote Sensing of Environment*, 233, 111325, <https://doi.org/10.1016/j.rse.2019.111325>, 2019.
- Raney, R. K. and Leuschen, C.: Technical Support for the Deployment Of Radar and Laser Altimeters during LaRA 2002, 535 Final Report, 21, 2003.
- Ricker, R., Hendricks, S., Helm, V., Skourup, H., and Davidson, M.: Sensitivity of CryoSat-2 Arctic sea-ice freeboard and thickness on radar-waveform interpretation, *The Cryosphere*, 8, 1607–1622, <https://doi.org/10.5194/tc-8-1607-2014>, 2014.
- Ricker, R., Fons, S., Jutila, A., Hutter, N., Duncan, K., Farrell, S. L., Kurtz, N. T., and Fredensborg Hansen, R. M.: Linking scales of sea ice surface topography: evaluation of ICESat-2 measurements with coincident helicopter laser scanning during 540 MOSAiC, *The Cryosphere*, 17, 1411–1429, <https://doi.org/10.5194/tc-17-1411-2023>, 2023.
- Rotermund, L. M., Williams, W. J., Klymak, J. M., Wu, Y., Scharien, R. K., and Haas, C.: The Effect of Sea Ice on Tidal Propagation in the Kitikmeot Sea, Canadian Arctic Archipelago, *Journal of Geophysical Research: Oceans*, 126, e2020JC016786, <https://doi.org/10.1029/2020JC016786>, 2021.
- Tilling, R. L., Ridout, A., and Shepherd, A.: Estimating Arctic sea ice thickness and volume using CryoSat-2 radar altimeter 545 data, *Advances in Space Research*, 62, 1203–1225, <https://doi.org/10.1016/j.asr.2017.10.051>, 2018.
- Ullaby, F. T., Moore, R. K., and Fung, A. K.: Microwave Remote Sensing. Active and Passive., *Geological Magazine*, 124, 88–88, <https://doi.org/10.1017/S0016756800015831>, 1987.



- Warren, S. G., Rigor, I. G., Untersteiner, N., Radionov, V. F., Bryazgin, N. N., Aleksandrov, Y. I., and Colony, R.: Snow Depth on Arctic Sea Ice, *Journal of Climate*, 12, 1814–1829, [https://doi.org/10.1175/1520-0442\(1999\)012<1814:SDOASI>2.0.CO;2](https://doi.org/10.1175/1520-0442(1999)012<1814:SDOASI>2.0.CO;2), 1999.
- Webster, M., Gerland, S., Holland, M., Hunke, E., Kwok, R., Lecomte, O., Massom, R., Perovich, D., and Sturm, M.: Snow in the changing sea-ice systems, *Nature Clim Change*, 8, 946–953, <https://doi.org/10.1038/s41558-018-0286-7>, 2018.
- Webster, M. A., Rigor, I. G., Nghiem, S. V., Kurtz, N. T., Farrell, S. L., Perovich, D. K., and Sturm, M.: Interdecadal changes in snow depth on Arctic sea ice, *Journal of Geophysical Research: Oceans*, 119, 5395–5406, <https://doi.org/10.1002/2014JC009985>, 2014a.
- Willatt, R., Laxon, S., Giles, K., Cullen, R., Haas, C., and Helm, V.: Ku-band radar penetration into snow cover on Arctic sea ice using airborne data, *Ann. Glaciol.*, 52, 197–205, <https://doi.org/10.3189/172756411795931589>, 2011.
- Xu, C., Mikhael, W., Myers, P. G., Else, B., Sims, R. P., and Zhou, Q.: Effects of Seasonal Ice Coverage on the Physical Oceanographic Conditions of the Kitikmeot Sea in the Canadian Arctic Archipelago, *Atmosphere-Ocean*, 59, 214–232, <https://doi.org/10.1080/07055900.2021.1965531>, 2021.
- Yackel, J., Geldsetzer, T., Mahmud, M., Nandan, V., Howell, S. E. L., Scharien, R. K., and Lam, H. M.: Snow Thickness Estimation on First-Year Sea Ice from Late Winter Spaceborne Scatterometer Backscatter Variance, *Remote Sens.*, 11, 417, <https://doi.org/10.3390/rs11040417>, 2019.
- Zheng, J., Geldsetzer, T., and Yackel, J.: Snow thickness estimation on first-year sea ice using microwave and optical remote sensing with melt modelling, *Remote Sens. Environ.*, 199, 321–332, <https://doi.org/10.1016/j.rse.2017.06.038>, 2017.

Appendix A

570 **Table A1: Geophysical corrections applied on the IS2 ATL07 product. The range represents the typical variation in the corrections as reported in the IS2 Algorithm Theoretical Basis Document (ATBD).**

Geophysical Correction	Typical Range	Source
Solid Earth Tide	-19 to +27 cm	IERS 2010 (Applied in ATL03)
Solid Earth Pole Tides	-0.6 to +0.7 cm	IERS 2010 (Applied on ATL03)
Ocean Pole tides	+/- 2 mm	IERS 2010 (Applied in ATL03)



Ocean loading	-9.7 to +9.3 cm	GOT4.8 Ocean Tide Model (Applied in ATL07)
Ocean Tides	-6.2 to +6.2 m	GOT4.8 Ocean Tide Model (Applied in ATL07)
Long period equilibrium tides	-7.1 to +6.0 cm	GOT4.8 Ocean Tide Model (Applied in ATL07)
Inverted barometer	-53 to +94 cm	ATL09/GEOS5 FP-IT (Applied in ATL07)

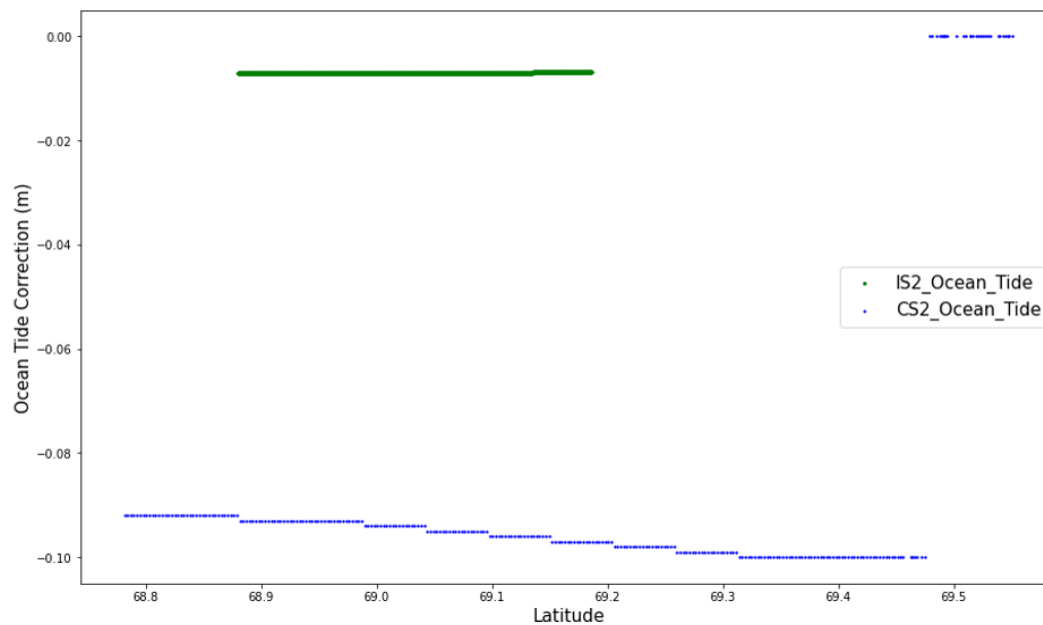
Appendix B

575 **Table B1: Geophysical Corrections applied in the CS2 Level 2 product. The typical range values are reported in the Cryosat-2 Baseline E Level 2 Product Handbook.**

Geophysical Correction	Typical Range	Source
Ocean Tide	-50 to +50 cm	Finite Element Solution FES 2004 Tide Model
Long-Period Equilibrium Ocean Tide	< 1cm	Finite Element Solution FES 2004 Tide Model
Ocean Loading	-2 to +2 cm	Finite Element Solution FES 2004 Tide Model
Solid Earth Tide	-30 to +30 cm	Cartwright Tide model (Cartwright & Edden, 1973)
Geocentric Polar Tide	-2 to +2 cm	Historical Pole Positions from CNES
Inverted Barometer	-15 to +15 cm	Dynamic Surface Pressure from Meteo France



Appendix C



580

Figure C1: Ocean tidal correction used in the IS2 and CS2 tracks. The IS2 ocean tide corrections are shown in green while the CS2 ocean tide corrections are shown in blue.

585